NASA TECHNICAL NOTE

NASA TN D-6636

NOISE PRODUCED BY A SMALL-SCALE, EXTERNALLY BLOWN FLAP

by William A. Olsen, Robert G. Dorsch, and Jeffrey H. Miles

Lewis Research Center
Cleveland, Ohio 44135

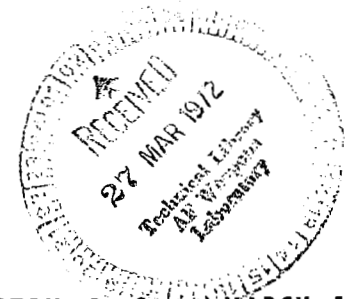

NATIONAL AERONAUTICS AND SPACE ADMINISTRATION • WASHINGTON, D. C. • MARCH 1972

1. Report No. NASA TN D-6636	2. Government Accession No.	3. Recipient's Catalog No.

4. Title and Subtitle	5. Report Date
NOISE PRODUCED BY A SMALL-SCALE, EXTERNALLY BLOWN FLAP	March 1972
	6. Performing Organization Code

7. Author(s)	8. Performing Organization Report No.
William A. Olsen, Robert G. Dorsch, and Jeffrey H. Miles	E-6662
	10. Work Unit No. 764-72
9. Performing Organization Name and Address	11. Contract or Grant No.
Lewis Research Center National Aeronautics and Space Administration Cleveland, Ohio 44135	13. Type of Report and Period Covered Technical Note
12. Sponsoring Agency Name and Address	14. Sponsoring Agency Code
National Aeronautics and Space Administration Washington, D.C. 20546	

15. Supplementary Notes

16. Abstract

Noise data were obtained with a model of an externally blown flap of the type that is currently being considered for STOL aircraft. The noise caused by impingement of the jet on the flap is much louder than the nozzle jet noise. It is especially so directly below the wing. The noise level increases as the jet velocity and flap angle are increased. The sound power level increased with the sixth power of velocity. Several physical variations to this STOL model configuration were also tested. Two such variations, a large board and a slotless curved plate wing, had the same power spectral density (Strouhal number curve) as the model.

17. Key Words (Suggested by Author(s))

Short-takeoff aircraft
V/STOL aircraft
Noise (sound)
Jet-impingement noise
(Jet) aircraft noise
Aerodynamic noise

18. Distribution Statement

Unclassified - unlimited

19. Security Classif. (of this report)	20. Security Classif. (of this page)	21. No. of Pages	22. Price*
Unclassified	Unclassified	38	$3.00

* For sale by the National Technical Information Service, Springfield, Virginia 22151

CONTENTS

	Page
SUMMARY	1
INTRODUCTION	1
APPARATUS AND PROCEDURE	2
Flow System	2
Valve Noise Quieting	2
Test Models	3
Basic configuration	3
Variations to the basic configuration	3
Acoustic Instrumentation	4
Test Procedure	4
RESULTS AND DISCUSSION	5
Basic Configuration	5
Noise radiation patterns above and below the wing	5
Azimuthal variation of the noise radiation pattern	6
Sound pressure level spectra at $\theta_m = 100^o$	7
Sound power level spectra	8
Variation of noise with jet velocity	8
Strouhal plots	9
Variations to the Basic Configuration	10
Slotless wing and board	10
Nozzle at other positions	11
No jet impingement on the 0^o flap	11
Larger nozzle at same thrust	12
Dominant internal noise	12
Aerodynamic Measurements	12
SUMMARY OF RESULTS	13
APPENDIX - SYMBOLS	15
REFERENCES	16

NOISE PRODUCED BY A SMALL-SCALE, EXTERNALLY BLOWN FLAP

by William A. Olsen, Robert G. Dorsch, and Jeffrey H. Miles

Lewis Research Center

SUMMARY

Noise data were obtained with a model of an externally blown flap of the type that is currently being investigated for STOL aircraft. The noise generated by impingement of the jet on the externally blown flap at the 30°-60° flap position is considerably louder (more than 10 dB) than the noise caused by the nozzle jet alone. It is especially loud below the wing. As the flap angle is decreased from the 30°-60° flap position to the 10°-20° flap position, and finally to the fully retracted (0°) flap position, the noise generated decreases. The noise is generally lower on the sideline than below the wing. The sound power level generated by impingement of the jet on the 30°-60° flap increased with the sixth power of this velocity. As the nozzle jet velocity increased, the sound power level of noise from the nozzle alone increased with the eighth power of the jet velocity. Therefore, the difference between the impingement noise and the noise of the nozzle alone decreased with increasing velocity. The noise radiation pattern above and below the 30°-60° flap position changed its shape only slightly as the jet pressure ratio (velocity) decreased.

Several variations of the blown flap model were also tested. The jet was blown against a slotless metal wing and against a very large, flat board. Comparison of these noise radiation patterns with those for the blown flap (at the 30°-60° position) suggests that the noise is generated by jet impingement on the curved surfaces and by the jet wake leaving the wing. The frequency distributions of the noise generated by the model wing and the two variations were similar.

Noise data were also taken for another group of variations which involved changes in the nozzle position relative to the wing and flap and changes in the nozzle. All of these variations showed that the noise increased with increased impingement velocity.

INTRODUCTION

Short takeoff and landing (STOL) aircraft require some form of lift augmentation during landing and takeoff. One of the proposed lift-augmentation methods is the extern-

ally blown flap, where the engine exhaust jet is deflected downward by trailing-edge flaps. STOL aircraft are designed to take off and land near heavily populated areas. Therefore, the noise they generate during those operations must stay below acceptable limits. The impingement and turning of the engine exhaust jet by the flap result in additional noise below the aircraft. This additional noise may become the dominant noise source if a quiet engine is employed.

As part of the aeronautical research program at the Lewis Research Center, the noise generated by several STOL lift-augmentation methods is being studied (e.g., ref. 1). This report contains the results of an investigation of the noise generated by a small model (32-cm chord) of a double-slotted, externally-blown flap. It is similar to one of the STOL wing configurations developed by the Langley Research Center (ref. 2). Variations to this configuration were also tested.

Far field noise data for three flap positions and for the nozzle alone are presented for selected nozzle pressure ratios between 1.1 and 2.2. Emphasis was placed on noise measurements in the plane perpendicular to the wing. Limited measurements of the azimuthal variation of noise about the nozzle centerline were also taken. Basic flow data such as velocity profile measurements in the vicinity of the flaps are given.

APPARATUS AND PROCEDURE

Flow System

The flow system (fig. 1) was attached to the laboratory air supply. It consisted of the following (proceeding downstream): an orifice for flow measurement; a 10-centimeter globe flow-control valve; a valve-noise-quieting section; a long straight run of 10-centimeter-diameter pipe; and finally, the convergent nozzle. The nozzle jet was directed at the wing-and-flap configuration. Depending on the season, the nozzle stagnation temperature varied from 273 to 300 K.

Valve Noise Quieting

The total sound power level PWL'_T (symbols defined in the appendix) of the noise generated by the unquieted flow-control valve was about 140 decibels and was loudest above a frequency of 1 kilohertz. The sound power level produced by the exhaust jet from a 5.2-centimeter test nozzle at the lowest nozzle pressure ratio of this experiment is lower than this. For this worst case, valve noise must be reduced by at least 30 decibels in order to obtain correct jet-noise data. This attenuation requirement was

achieved by the valve-noise-quieting section shown in figure 1. The first valve-quieting elements downstream of the valve were two perforated plates. A 10-percent-open-area perforated plate (hole diam, 0.2 cm) was attached to the valve exit flange and was followed by a 1-centimeter spacer, and then by a 15-percent-open-area perforated plate (hole diam, 0.95 cm). A dissipative muffler (attenuation greater than 20 dB from 2 to 6.3 kHz) was located downstream of the perforated plates. The quieting section performed as required. Its performance is discussed further in a later section.

Test Models

Basic configuration. - A cross-sectional view of the small-scale model (32-cm wing chord) of the externally blown flap system is shown in figure 2. It is similar to the STOL wing configuration described in reference 2. The model arrangement shown in figure 2, which was used to provide three different flap positions, is herein called the basic configuration. The three flap positions tested were 30°-60°, 10°-20°, and 0° (retracted). The 30°-60° flap notation refers to a leading flap angle of 30° and a trailing flap angle of 60° down from the mean chord line of the wing. Figure 3 is a photograph of the model in the 30°-60° flap position. The wing and flaps were made of wood covered with fiber glass and were smooth and polished. The wing-and-flap assembly was secured rigidly to the inlet pipe by rotatable clamps. The wing and flaps were bolted to small end plates so that the three flap positions could be achieved simply.

Variations to the basic configuration. - Noise data were also taken for some variations to the basic configuration. The purpose of these tests was to determine the effect of configuration changes on the noise generated and to provide some insight into the mechanism of blown-flap noise generation and its distribution.

Figure 4(a) shows two variations to the basic configuration of the 30°-60° flap. In one, the wing and flaps were replaced by a solid aluminum plate cut and rolled to conform to the smoothed lower boundary of the 30°-60° flap. The other variant was a large, flat board ($2\frac{1}{2}$ m square) placed at 60° to the nozzle centerline.

In the basic configuration, the nozzle and wing are positioned as shown in figure 2. The nozzle was also placed at other locations (i.e., different H and L_L dimensions in fig. 2) relative to wing at the 30°-60° flap position.

In the basic configuration, there is some jet impingement even when the flap is in the 0° flap (retracted) position. Therefore, for another variation, the wing was moved further away from the nozzle centerline, as shown in figure 4(b). But in order to get good flow around the wing flaps when in this position, the jet must be directed somewhat upward. The deflector plate shown in figure 4(b) was used to turn the jet.

Figure 4(c) shows the arrangement for the simulation of a larger engine of the same thrust (but lower velocity). A 7.8-centimeter nozzle was used. The nozzle centerline was located farther from the wing so that the jet impingement area on the wing was about the same as for the 5.2-centimeter nozzle in the basic configuration.

In addition to these geometrical variations, the basic configuration was run once with a dominant internal noise source. This internal noise was generated by a 2.2-centimeter-diameter orifice upstream of the nozzle. This last variation would be grossly equivalent, so far as noise is concerned, to an engine whose fan noise was higher than its jet noise or any jet impingement noise.

Acoustic Instrumentation

The noise data were measured with fourteen, 1.27-centimeter (0.5-in.), condenser microphones with windscreens. The microphones were located in a horizontal plane which passed through the nozzle centerline. The nozzle centerline was 1.22 meters above a smooth, flat, asphalt surface. The microphones were placed on a 3.04-meter-radius circle (see fig. 5) at 20° intervals on the nozzle (noisy) side of the wing and at 20° to 30° intervals on the other side of the wing. The angle $\theta_m = 0^{\circ}$ is in the direction of the nozzle jet.

Most of the noise data were taken with the wing vertical ($\varphi_w = 0^{\circ}$, in fig. 5). Therefore, those data would be indicative of the noise distribution below and above the proposed STOL aircraft. The wing-and-flap assembly was rotated about the nozzle centerline to determine the variation of the noise about this line (i.e., variation with φ_w). The sideline noise distribution was measured at $\varphi_w = 85^{\circ}$ to avoid the shadow of the end plates (see fig. 3).

Test Procedure

Far field noise and flow data were taken for as many as five nominal nozzle pressure ratios (P_R = 1.1, 1.25, 1.4, 1.7, and 2.25) for each configuration and for the nozzle alone. The test configurations, nominal nozzle pressure ratios, and nozzle exhaust jet velocities for each run are listed in table I.

The microphones were kept out of the exhaust jet for most of the data. Late in the test program, they were placed in the slower parts of the exhaust stream to fill in gaps in the radiation patterns. The spectra for these microphones (with windscreens) were easily corrected for the jet "wind" noise resulting from their placement in the exhaust stream, because that noise occurs at much lower frequency than does the data noise.

Three noise data samples were taken at each microphone location for each run condition. Twenty minutes were required for three samples of data for the 14 microphones. Noise data were analyzed directly by a one-third octave band spectrum analyzer. The analyzer determined sound pressure level spectra in decibels referenced to 2×10^{-5} N/m^2 (0.0002 microbar). The three samples were then arithmetically averaged, and a correction was applied for the microphone, cable, and atmosphere losses. No spectral corrections were deemed necessary for ground reflections because the major cancellations and reinforcements occur at much lower frequencies than the region of interest. The overall sound pressure level at each microphone position was computed from the averaged and corrected spectra. The power spectrum and total power were computed by a spatial integration of the averaged and corrected spectral data from each microphone. The integration was performed by using the spherical-geometry area elements shown in figure 5. Because the values of sound pressure level at each microphone angle θ_m already include the ground reflection contribution, the integration for power is made over a hemisphere.

The condenser microphones were calibrated before each day of testing with a standard piston calibrator (a 124-dB, 250-Hz tone). The one-third octave band analyzer was calibrated before the test with a constant voltage source and was checked during the experiment with an electronic pink noise generator. The data-acquisition and the data-analysis systems were further checked with an orifice noise source. The noise level produced by this source was repeatable to within approximately $1\frac{1}{2}$ decibels. Considering these calibrations and checks, the redundant data, and the averaging of three samples widely spaced in time, it is estimated that the reported data are repeatable from day to day to within $1\frac{1}{2}$ decibels. Much of the directly compared data were obtained on the same day, so that these data are repeatable to within approximately 1/2 decibel.

RESULTS AND DISCUSSION

The noise data obtained in this investigation are summarized in figure form. For those requiring more detail, complete tables of the one-third octave noise spectra obtained are available, on request, from the authors.

Basic Configuration

Noise radiation patterns above and below the wing. - STOL aircraft are expected to steeply ascend from or descend to small airports near populated areas. Consequently, the important noise measurements are those below the aircraft. Figure 6 shows the noise radiation patterns in the plane perpendicular to the wing ($\varphi_w = 0^o$, in fig. 5). The curves in figure 6(a) are for the 30^o-60^o flap of the basic configuration at nominal nozzle

pressure ratios P_R of from 1.1 to 2.25. The overall sound pressure level, OASPL, clearly increases with nozzle pressure ratio (or nozzle exhaust velocity). The noise is greatest under the wing and least above it. For example, at $P_R = 1.7$, the noise is 8 decibels greater directly below the wing than directly above it. Further, the shapes of the noise radiation patterns for the 30^o-60^o flap are fairly similar over the range of pressure ratios used in the tests. At the higher pressure ratios, the peak noise occurs at roughly $\pm 30^o$ from the exhaust stream leaving the flap (hereinafter called the flap exhaust). At the low pressure ratios, the peak is about 90^o from the exhaust. The small amount of data taken within the jet exhaust region at $P_R = 1.7$ is plotted with solid symbols. The shapes of the faired curves in this region were estimated for the other pressure ratios. The estimates were based on the data obtained at $P_R = 1.7$ and data obtained for the 0^o flap.

Figures 6(b) and (c) show the noise radiation patterns for the 10^o-20^o flap and the retracted (0^o) flap, respectively. The shapes of these curves change with nozzle pressure ratio because of the influence of the nozzle jet noise on the total noise measured. The noise radiation patterns for the nozzle alone are shown in figure 6(d). These curves are similar, except for the curve for $P_R = 2.25$. This curve has a bump between $\theta_m = 90^o$ and $\theta_m = 270^o$ that is due to broadband shock noise (ref. 3).

The data curves of figure 6 are reorganized in figure 7 to show the effect of flap position on the radiation pattern. The curves for nozzle pressure ratios of 1.25, 1.7, and 2.25 are given in figures 7(a) to (c), respectively. The noise level clearly increases with flap angle at all pressure ratios. Figure 7 also shows that the separation between the flap noise and the noise of the nozzle alone decreases with increasing P_R. At $P_R = 1.7$ (fig. 7(b)), the noise caused by the 30^o-60^o flap is at least 10 decibels greater than the noise generated by the nozzle alone for nearly all values of θ_m. This means that the noise caused by the nozzle alone contributes less than 1/2 decibel to the total noise caused by the jet and jet impingement on the 30^o-60^o flap. At $P_R = 1.25$ (fig. 7(a)), the nozzle jet noise is a relatively minor contributor for even the 0^o and the 10^o-20^o flap settings. Conversely, at $P_R = 2.25$ (fig. 7(c)), the nozzle jet noise is important for both the 0^o and the 10^o-20^o flap settings.

Azimuthal variation of the noise radiation pattern. - The data in the previous section were taken with the wing and flaps perpendicular to the microphone circle plane ($\varphi_w = 0^o$). The resulting noise radiation patterns represent the overall sound pressure levels below and above the wing. The sideline noise radiation pattern, in the plane of the wing ($\varphi_w = 90^o$, in fig. 5), is also important. Sideline data were obtained by rotating the wing-and-flap assembly about the nozzle centerline to $\varphi_w = 85^o$. In this approximate sideline orientation ($\varphi_w = 85^o$), the flap exhaust is directed upward, away from the ground. Figure 8 shows the radiation pattern at $\varphi_w = 85^o$ for the 30^o-60^o, 10^o-20^o, and 0^o flap positions of the basic configuration at $P_R = 1.7$. In comparison with the $\varphi_w = 0^o$ case (fig. 7(b)), it is clear that less noise is radiated in the sideline plane.

The wing-and-flap assembly, at the 30^{o}-60^{o}, 10^{o}-20^{o}, and 0^{o} flap positions, was also rotated to other φ_w angles to determine the azimuthal variation of the noise radiation pattern. The difference between the OASPL at $\varphi_w = 0^{o}$ and the OASPL at various other values of φ_w for some selected microphone positions, θ_m, is plotted in figure 9. This figure presents curves of this difference ((OASPL at $\varphi_w = 0^{o}$) - (OASPL at φ_w)) for each flap position of the basic configuration at $P_R = 1.7$. It is apparent that this difference is roughly a linear function of φ_w. This linear variation reduces the amount of data necessary to determine the effect of varying φ_w. But as figure 9 shows, the difference is not a simple function of either θ_m or of the flap position. Figure 9 also indicates that for all flap positions, the sideline ($\varphi_w = 85^{o}$) noise is quieter than the noise in the $\varphi_w = 0^{o}$ plane for most microphone positions θ_m. Exceptions occur at $\theta_m = 40^{o}$ and at $\theta_m = 210^{o}$, where the 30^{o}-60^{o} flap is about 2 decibels louder.

Sound pressure level spectra at $\theta_m = 100^{o}$. - In order to determine the perceived noise level below and at the sideline of the aircraft, it is necessary to know the sound pressure level spectrum there. Figure 10 shows the one-third octave sound pressure level spectrum at $\theta_m = 100^{o}$ and $\varphi_w = 0^{o}$ for each flap position of the basic configuration for three nozzle pressure ratios. The choice of $\theta_m = 100^{o}$ for figure 10 is a compromise between being near the peak noise location and being near $\theta_m = 90^{o}$ from the standpoint of flyover noise.

The 0^{o} flap case is nearly equivalent to the common configuration for an engine pod mounted below an aircraft wing. Placing the 30^{o}-60^{o} flap in the nozzle exhaust adds about 10 decibels to the 0^{o} flap noise measured below the wing for frequencies above 1 kilohertz. This gives an appreciation of the increase in noise that would result below the wing of an externally-blown-flap STOL aircraft in comparison with a conventional aircraft.

Next, compare figures 10(a) to (c) for the frequency at which the peak noise occurs for the three flap positions. For the 30^{o}-60^{o} flap at $\theta_m = 100^{o}$, this frequency occurs at about 2, 2.5, and 3.15 kilohertz for $P_R = 1.25$, 1.7, and 2.25, respectively. This peak occurs at a lower frequency for the 10^{o}-20^{o} flap. Notice also in this comparison that the separation between the noise of the nozzle alone and the flap noise decreases with increasing P_R, especially at high and very low frequencies. The smaller separation at $P_R = 2.25$ above 5 kilohertz in figure 10(c) and also between 90^{o} and 270^{o} in figure 7(c) is caused by the presence of broadband shock noise in the data for the nozzle alone. This extra noise at supersonic pressure ratios was sufficient to markedly affect the noise measured for the 0^{o} and the 10^{o}-20^{o} flap positions (i.e., compare fig. 7(b) with 7(c)).

Figure 11 presents a plot of the sideline wing tip noise spectrum at $\theta_m = 100^{o}$ and $\varphi_w = 85^{o}$ for $P_R = 1.7$. The additional noise caused by impingement on the wing and flap is considerably less in the sideline direction.

Sound power level spectra. - The wing and flap affect the noise measured in essentially two ways. They redistribute (by reflection and shielding) the noise generated by the nozzle jet and any internal noise which might be present, and they generate additional noise. To get some idea of their separate contributions, the power spectrum (PWL) must be considered, because it is not affected by noise redistribution. Sufficient measurements were made of the azimuthal variation of noise (SPL spectrum as a function of θ_m and φ_w) to determine PWL, but only at $P_R = 1.7$. The azimuthal noise distribution, as evidenced by figure 9, was by no means axisymmetric. Therefore, the integration with φ_w, required for the power spectrum, cannot be evaluated in all cases. Instead, a measure of the power spectrum (PWL') is computed from the data measured in a single plane (e.g., at $\varphi_w = 0^o$). The integration is performed by assuming that there is no variation with φ_w from the data measured at a given φ_w. Figure 12(a) is a plot of PWL', evaluated at $\varphi_w = 0^o$, for each flap position of the basic configuration at $P_R = 1.7$. The peak noise power for the 30^o-60^o flap occurs at 2 kilohertz. Figure 12(b) is a similar plot, but it is evaluated from the sideline data at $\varphi_w = 85^o$. Figure 12 indicates that considerable noise power is generated by the impingement of the jet (i.e., the wing and flap do not just simply redirect the nozzle noise).

Throughout the noisier part of the spectrum, the noise power measured for the 30^o-60^o flap is about 12 decibels greater than the noise of the nozzle alone at $P_R = 1.7$ and $\varphi_w = 0^o$. This means that for this case, the nozzle noise makes no essential contribution (less than 1/2 dB) to the noise generated by jet impingement. The nozzle noise becomes an appreciable part of the total noise for the 0^o flap and the 10^o-20^o flap at high nozzle pressure ratios.

Variation of noise with jet velocity. - The distance L_T along the centerline from the exit plane of the nozzle to the impingement point on the wing-and-flap surface and the nozzle diameter D_N were held constant for the data taken for the basic configuration. From reference 4, the velocity profile downstream of a circular nozzle is given by the following functional relation:

$$\frac{u}{V_j} = F\left\langle \frac{r}{\frac{D_N}{2}}, \frac{x}{D_N} \right\rangle$$

But in this experiment, $x = L_T$ = a constant, and D_N is also a constant. Therefore, the impingement velocity would be proportional to the jet velocity V_j; and the impingement area would be proportional to the nozzle area.

From reference 5, it seems reasonable to assume that the total sound power of jet impingement noise would be a function of the impingement velocity, angle, and area, or in this case of V_j, D_N, and flap position. Figure 13 is a plot of the measure of total

sound power PWL'_T as a function of V_j for the flap configurations and for the nozzle alone. The data for the nozzle are approximately fitted by a V_j^8 curve for PWL'_T greater than 110 decibels. Below that noise power level, the valve noise of the facility that has not been attenuated becomes significant, and the eighth-power law is no longer followed. Actually, a V_j^9 curve would fit the data for the nozzle alone better than does the traditional V_j^8 curve for P_R between 1.25 and 2.25. The noise data for the 30^o-60^o flap of the basic configuration fall along a V_j^6 line. Because of less separation, the 0^o flap and perhaps even the 10^o-20^o flap might be expected to be influenced by the eighth-power nozzle noise. However, within the scatter of the data, they also seem to follow the sixth-power law reasonably well, except at high velocity.

Figure 14 is a plot of overall sound pressure level OASPL below the wing at $\theta_m = 100^o$ and $\varphi_w = 0^o$ as a function of V_j for all the flap positions. A V_j^6 line passes through these data for the basic configuration also.

Strouhal plots. - It has been well established (see ref. 6) that the noise from subsonic nozzles of circular cross section is correlated by a dimensionless power spectral density, as a function of Strouhal number, fD_N/V_j. Figure 15 is such a plot where, based on reference 6, the dimensionless power spectral density DPSD is defined by the equation

$$DPSD = (PWL - PWL_T) + 10 \log_{10}\left(\frac{V_j}{\Delta f_b D_N}\right)$$

The data from this report for the nozzle alone are given in figure 15(a). The solid curves are envelopes enclosing the data reported by reference 6. The data for this report fall within these envelopes and have a peak noise Strouhal number of about 0.15. A similar correlation was attempted for the impingement only noise of the 30^o-60^o flap. In this case, the noise of the nozzle alone is a small contributor to the noise measured. Therefore, the measured values of PWL' and PWL'_T can be adequately used without correcting for nozzle noise. Based on the previous discussion, the jet velocity V_j and nozzle diameter D_N are used in this correlation. Figure 15(b) contains this plot for the basic configuration at four pressure ratios. The data are well correlated.

Variations to the Basic Configuration

Noise data were also taken for certain variations to the basic configuration in order to gain some insight into the noise generation mechanisms. They will also be helpful in estimating the effect of configuration changes on the blown-flap noise.

Slotless wing and board. - A solid, slotless wing was made by bending an aluminum plate to conform to the smoothed lower boundary of the 30°-60° flap position of the basic configuration (see fig. 4(a)). Another variation shown in figure 4(a) is a very large, flat board at a 60° angle to the jet. In all the cases shown in figure 4(a), the target point is at the same distance from the nozzle (L_T = 37 cm), and the same 5.2-centimeter nozzle was used. This means that the impingement velocity and area are essentially the same. The impinged surface shape is different. These variations are useful in understanding the sources of the noise for the following reasons. The slotless wing has no flap leading edges to generate noise and no slots to transmit noise through to the region above the wing. The exhaust jets leaving the basic configuration and the slotless wing have high velocities and, therefore, generate noise. The exhaust jet leaving the large flat board, however, is too slow to generate noise.

The noise data for the 30°-60° flap, the slotless wing, and the board are compared in figure 16. The noise from the nozzle alone is a small contribution to the total noise in all cases shown. The noise radiation patterns are presented in figure 16(a). A sharp peak noise lobe occurs at $\theta_m = 80^{\circ}$ for the slotless wing and the board. The peak noise for the 30°-60° flap occurs over a larger sector from $\theta_m = 80^{\circ}$ to $\theta_m = 140^{\circ}$. The OASPL at $\theta_m = 80^{\circ}$ is about the same for all three cases. Notice from figure 16(a) that there are two peak noise lobes for the slotless wing and for the 30°-60° flap. One peak occurs at $\theta_m = 20^{\circ}$ for both. The other peak occurs at $\theta_m = 80^{\circ}$ for the metal wing and between 80° and 160° for the 30°-60° flap. The board has only one peak noise lobe, at $\theta_m = 80^{\circ}$, and the noise falls off rapidly on the backside of the board. Since no noise can be generated by the jet leaving the edge of the board, it is apparent that the peak noise lobe at $\theta_m = 20^{\circ}$ for the slotless wing is caused by the exhaust wake. Furthermore, this jet wake generates much more noise than the jet of an equivalent nozzle. Figure 16(a) also shows that the slotless wing and the board generate less noise than does the basic configuration from $\theta_m = 90^{\circ}$ to $\theta_m = 180^{\circ}$. Apparently, jet impingement on the flap leading edges of the basic configuration generates additional noise and directs it toward the nozzle. The noise below the wing ($\theta_m = 90^{\circ}$) is due to the jet wake and impingement on the flap surfaces. The passage of noise through the slots in the basic configuration accounts for the higher noise levels above this wing than above the slotless wing.

Figure 16(b) is a plot of SPL one-third octave spectra at $\theta_m = 80^{\circ}$ for the 30°-60° flap and the two variations. The peak noise for all three cases falls between 2 and 3.15 kilohertz.

Noise data were taken for the slotless wing at the three nominal pressure ratios of this experiment. Figure 17 presents the noise radiation patterns for the slotless metal wing at P_R = 1.25, 1.7, and 2.25. These patterns are similar. The peak noise location moves to larger θ_m as P_R decreases, just as with the basic configuration (see

fig. 6(a)). The noise power (PWL'_T) data for the slotless wing, which are plotted in figure 13, fall along a V_j^6 line. The shift in the noise pattern with P_R affects the variation of OASPL with V_j for each θ_m. For example, the OASPL at 120^o follows a V_j^6 curve, but at 80^o it follows a V_j^8 curve.

The dimensionless power spectral densities for the basic configuration at the 30^o-60^o flap position, the slotless wing, and the flat board are plotted in figure 18. For these variations, the impingement velocity and area for a given P_R are essentially the same. Therefore, the nozzle jet velocity V_j and the nozzle diameter D_N are used, as before, as the scaling parameters. The slotless wing, the board, and the basic configuration at the 30^o-60^o flap position all fall on the same spectral curve.

Additional data were taken with the board inclined at 60^o from the nozzle centerline. It was blown upon by nozzles of varying size. The distance L_T between the nozzle and the board was varied so that $L_T/D_N = 7.05 = \text{constant}$. This assured the same impingement velocity for a given value of V_j. Since no noise is generated by the jet wake off the board, this comparison gives some indication of the effect of nozzle size on impingement noise. The noise level increased linearly with the nozzle exit area. Figure 19 is a dimensionless power spectral density plot of these data. Again, all the data fall along the same spectral curve.

Nozzle at other positions. - The externally blown flap configuration proposed for STOL aircraft uses a bypass engine. This bypass nozzle was approximated in the basic configuration by a single convergent nozzle placed at the fan nozzle exhaust position. Figure 20 is a plot at $P_R = 1.7$ of the difference between the OASPL at other nozzle positions (i.e., at other values of H and L_L) and the OASPL for the basic-configuration nozzle position. The solid curve indicates only a small OASPL difference between placing the nozzle at the core nozzle position and at the fan nozzle position of the basic configuration. The choice of nozzle position was, therefore, only important in achieving good flow around the flaps.

The other nozzle positions tested were all closer to the wing and flap than for the basic configuration. Therefore, they produced higher impingement velocities and were generally noisier, as evidenced by the data points of figure 20. For example, when the nozzle was moved so that it blew directly on the leading edge of the wing ($H = 1$ cm, and $L_L = 6.05$ cm), the noise level, OASPL, at $\theta_m = 100^o$ was almost 4 decibels higher than for the nozzle location of the basic configuration.

No jet impingement on the 0^o flap. - In the 0^o flap position of the basic configuration, the wing is at a position where there is some impingement of the jet on the surface of the wing. Therefore, some jet impingement noise should be expected. For comparison, the wing at the 0^o flap position was moved upward, away from the nozzle centerline, to avoid impingement (see fig. 4(b)). Figure 10(a) shows the noise spectra at $\theta_m = 100^o$ for the two nozzle positions with the 0^o flap. It is evident from this figure that for the basic configuration, jet impingement on the 0^o flap adds additional noise to the noise of

the nozzle alone. Reflection of the peak nozzle noise off the wing accounts for the separation between the SPL of the 0° flap without jet impingement and the SPL of the nozzle alone. To show this, consider figure 12(a), where the power spectra for these cases are plotted. These curves show a measure of the actual noise power generated, and they are essentially independent of reflection. From this figure, it is clear that no significant noise is generated by the no-jet-impingement location of the 0° flap, whereas significant noise is generated by the basic-configuration location of the 0° flap.

In order to get good lift augmentation at the 30°-60° flap position, with the wing raised to this no-impingement (on the 0° flap) position, the nozzle flow would have to be directed toward the wing. Therefore, when the wing was in this position, the jet was directed upward by using a deflector plate in the manner described in reference 7. Figure 21 shows that the noise generated by impingement of the jet on the deflector plate is much louder than the noise of the nozzle alone. But figure 21 also shows that the deflector plate adds only 1 or 2 decibels to the noise of the 30°-60° flap of the basic configuration, where no deflector was used.

Larger nozzle at same thrust. - A larger engine with a lower jet velocity was also simulated. The jet of a 7.8-centimeter nozzle at $P_R = 1.3$ was directed at the 30°-60° flap. This is about the same jet thrust as that produced by the 5.2-centimeter nozzle at $P_R = 1.7$. The centerline of the 7.8-centimeter nozzle was moved away from the wing as shown in figure 4(c) so that the upper impingement boundary of the jet on the wing was about the same as for the 5.2-centimeter nozzle. Figure 22 shows that the noise below the wing is about 7 decibels quieter for the larger nozzle.

Dominant internal noise. - Suppose, for example, that the fan-machinery noise in the exhaust jet of a bypass engine was much louder than the jet impingement noise. In such a case, the shape of the noise radiation pattern would be due to redirection of this internal noise by the wing-and-flap geometry. In an effort to gain insight into this redirection, a 2.2-centimeter-diameter orifice was installed upstream of the nozzle as an overpowering internal noise generator. This internal noise was dominant at high frequency. Figure 23 shows the noise patterns that were obtained with and without this overpowering internal noise for the 30°-60° flap and for the nozzle alone at a nozzle $P_R = 1.25$. The wing and flap do, indeed, simply redirect the dominant internal noise, which is much larger than the jet-impingement noise.

The peak noise for the nozzle alone, which occurred near $\theta_m = 20^{\circ}$ with no internal noise, moves to about $\theta_m = 50^{\circ}$ with a dominant internal noise.

Aerodynamic Measurements

A total-pressure rake and tufts were used to determine the magnitude and direction of the airflow around the flaps and in the downstream wake of the basic configuration.

The data were taken at the 30°-60° flap position at $P_R = 1.25$ and are summarized in figure 24. The total-pressure probes were internally chamfered to reduce sensitivity to the angle of flow. The rake was alined with the tufts. The direction of flow was obtained from photographs of the tuft direction. The flow was essentially tangent to the wing-and-flap surface. Figure 24(a) shows the location, vector direction, and magnitude of the velocity profile measurements on the nozzle side of the wing-and-flap surface. Figure 24(b) presents the results of similar measurements on the upper side of the wing and flaps. The velocity profiles downstream of the trailing flap are plotted in figure 24(c). From these data, it is evident that there is considerable spanwise flow at the 30°-60° flap position. It is also apparent that there are very large velocities and velocity gradients near the target point of the 30°-60° flap.

SUMMARY OF RESULTS

The following are the significant results for the externally blown flap model of the basic configuration:

1. The noise generated by the impingement of the jet on the wing and flap was considerably louder than the noise from the nozzle alone. The noise increases with increasing flap angle. The 30°-60° flap was more than 10 decibels noisier than the nozzle alone.

2. The sound power level of the flap noise and the overall sound pressure level below the wing increased with the sixth power of the jet velocity.

3. It was noisier below the wing than above it and less noisy along the sideline.

4. The noise radiation pattern above and below the 30°-60° flap changed its shape only slightly as the jet velocity (pressure ratio) changed. The pattern was less similar for the 10°-20° flap and the 0° flap positions because of the influence of the nozzle noise.

5. The azimuthal variation of the difference in overall sound pressure level was approximately a linear function of the azimuthal angle of the wing plane. But it was a complicated function of the flap angle and microphone angular location.

The following are the significant results for the variations of the basic configuration:

1. A comparison of the noise radiation patterns obtained with the 30°-60° wing flap, the slotless metal wing, and the large flat board suggests that the flap exhaust wake and the jet impingement on the flap leading edges are important noise contributors.

2. The frequency distributions of the noise generated by these three configurations were similar in that they fell on the same curve of power spectral density as a function of Strouhal number.

3. When the nozzle was moved to a position that was closer to the wing-and-flap surface than for the basic configuration, the flap noise increased, but no more than 6 decibels.

4. The flap noise for a larger diameter nozzle having lower exhaust velocity but the same thrust was significantly quieter.

Lewis Research Center,
National Aeronautics and Space Administration,
Cleveland, Ohio, December 7, 1971,
764-72.

APPENDIX - SYMBOLS

C_1, C_2, C_3	cancellation frequencies of ground reflection: fundamental and first and second harmonic, Hz
DPSD	dimensionless power spectral density, dB
D_N	nozzle diameter, cm
f	one-third octave band center frequency, Hz
Δf_b	one-third octave frequency band width, Hz
H	vertical distance from nozzle centerline to leading edge of wing, m
L_L	axial distance from nozzle lip to leading edge of wing, m
L_T	distance along nozzle centerline from nozzle exit to target point on wing flap, m
M_j	nozzle exit centerline Mach number, dimensionless
OASPL	overall sound pressure level, dB
$OASPL\langle \varphi_w \rangle$	overall sound pressure level in the φ_w plane, dB
P_R	nominal nozzle pressure ratio
PWL	sound power level, dB
PWL'	measure of sound power level, calculated from data at a given φ_w, dB
PWL'_T	measure of total power level, calculated from data at φ_w, dB
R_1, R_2, R_3	reinforcement frequencies of ground reflection, Hz
r	radial distance from nozzle centerline, m
SPL	sound pressure level, dB
u	exhaust axial velocity downstream of nozzle, m/sec
V_j	nozzle-exit centerline velocity, m/sec
x	distance downstream from nozzle exit, m
θ_m	angular location of microphones in horizontal plane (nozzle exhaust is at $\theta_m = 0^o$), deg
φ_w	azimuthal angle; angle of model wing plane from vertical plane of the experiment, deg

REFERENCES

1. Dorsch, R. G.; Krejsa, E. A.; and Olsen, W. A.: Blown Flap Noise Research. Paper 71-745, AIAA, June 1971.

2. Freeman, Delma C., Jr.; Parlett, Lysle P.; and Henderson, Robert L.: Wind-Tunnel Investigation of a Jet Transport Airplane Configuration with an External-Flow Jet Flap and Inboard Pod-Mounted Engines. NASA TN D-7004, 1970.

3. Simcox, C. D.: Studies of Shock Related Noise Fields Generated by Hot and Cold Choked Jets. Rep. D6-24486, Boeing Company, Oct. 1969.

4. Dealy, J. M.: The Confined Circular Jet with Turbulent Source. ASME Fluids Engineering Division Conference, Symposium on Fully Separated Flows. Arthur G. Hansen, ed., ASME, 1964, pp. 84-91.

5. Gordon, Colin G.: A Study of Exhaust Noise as it Relates to the Turbofan Engine. Progress of NASA Research Relating to Noise Alleviation of Large Subsonic Jet Aircraft. NASA SP-189, 1968, pp. 319-334.

6. Howes, Walton L.: Similarity of Far Noise Fields of Jets. NASA TR R-52, 1960, pp. 132-134.

7. Maglieri, Domenic J.; and Hubbard, Harvey H.: Preliminary Measurements of the Noise Characteristics of Some Jet-Augmented-Flap Configurations. NASA Memo 12-4-58L, 1959.

TABLE I. - EXPERIMENTAL TEST CONFIGURATIONS, NOMINAL PRESSURE RATIOS, AND JET VELOCITIES

Run	Azimuthal angle, φ_w, deg	Configuration					Nominal nozzle pressure ratio, P_R	Nozzle exhaust velocity, V_j, m/sec
		Description	Flap position, deg	Nozzle diameter, D_N, cm	Vertical distance from nozzle centerline to leading edge of wing, H, cm	Axial distance from nozzle lip to leading edge of wing, L_L, cm		
83	(a)	Nozzle alone	(a)	5.2	(a)	(a)	2.25	344
76							1.25	190
81							1.25	195
80							1.7	292
54							1.7	283
22							2.78	384
82							1.1	130
20							2.25	343
50							1.4	236
78		Nozzle alone with deflector plate					1.7	290
53		Nozzle alone with 2.2-cm orifice upstream for internal noise					1.25	194
127		Nozzle alone		7.8			1.3	200
49	0	Basic configuration	0	5.2	7.8	6.05	2.25	343
94							1.25	190
93							1.4	231
91							1.7	282
71								286
72	30							
73	60							
74	85							
75	0	Basic configuration with no jet impingement			12.5			
100		Basic configuration	10-20	5.2	7.8	6.05	1.25	190
101							1.7	282
57							2.25	341
56							1.25	194
55							1.7	283
128								279
131	30							
130	60							
129	85							
122	0	Basic configuration	30-60	5.2	7.8	6.05	1.25	186
102							1.7	282
95							1.7	282
97							1.4	231
98							1.25	190
84							2.25	344
42							2.25	341
121							1.1	130
39							1.7	285
43	30							
44	60							
45	85							
77	0	Basic configuration but at no jet impingement for 0° flap			12.5			288
52	0	Basic configuration with 2.2-cm orifice upstream for internal noise			7.8		1.25	195
118	0	Slotless metal wing	(b)	5.2	7.8	6.05	1.7	285
117	0	Slotless metal wing	(b)	5.2	7.8	6.05	1.25	186
119	0	Slotless metal wing	(b)	5.2	7.8	6.05	2.25	338
155	0	Basic configuration	30-60	5.2	7.8	6.05	1.7	294
156		Nozzle position closer to wing			7.8	[c] -2.54		
162					7.8	[c] -12.75		
163					[c] 3.0	6.05		
164					[c] 1.0	6.05		
126				7.8	[c] 9.0	6.05	1.3	200
97	0°	Flat board at 60° angle of impingement and L_T/D_N = 7.05	N/A	5.2	N/A	N/A	1.7	278
96				5.2			1.25	183
113				4.1			1.7	278
112				4.1			1.25	183
136				2.7			1.25	183
114				7.8			1.25	200

[a] No wing or flap used.
[b] Slotless metal wing contoured like lower surface of wing with 30°-60° flap.
[c] See fig. 2.

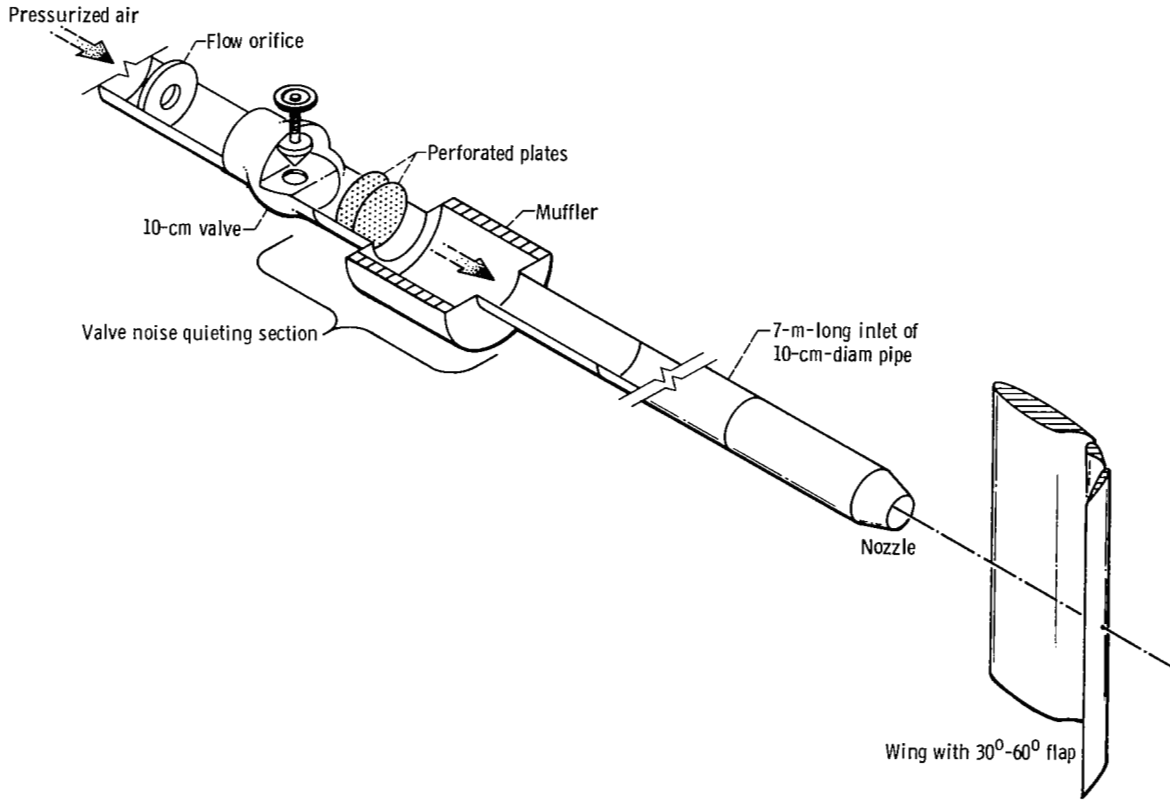

Figure 1. - Flow system.

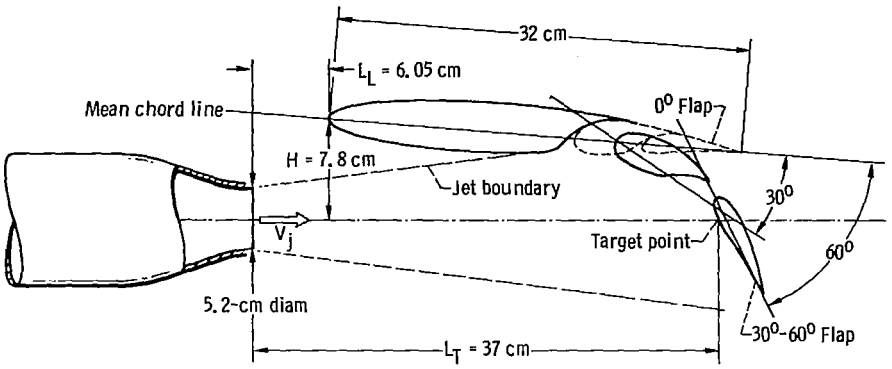

Figure 2. - Basic configuration of externally blown flap model.

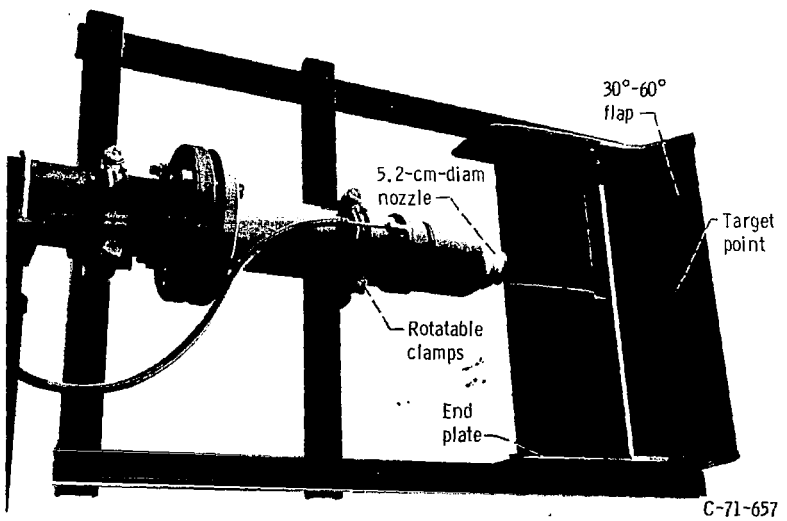

Figure 3. - Basic configuration.

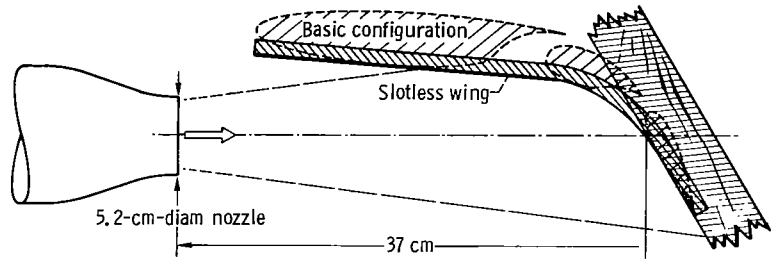

(a) Large flat board and slotless wing.

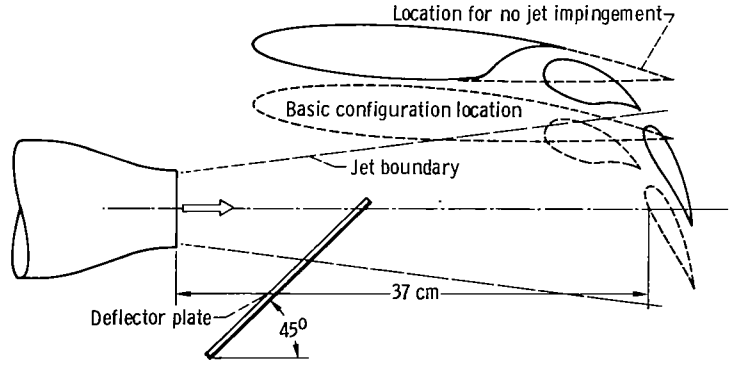

(b) Wing location to avoid jet impingement on 0° flap. Also shown is the deflector plate variation used with the 30°-60° flap at that location.

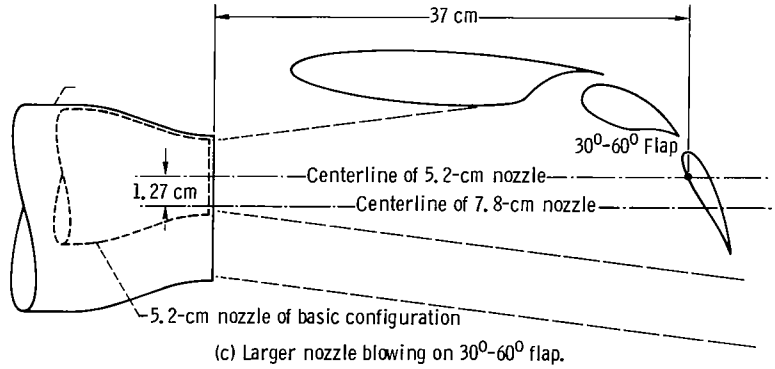

(c) Larger nozzle blowing on 30°-60° flap.

Figure 4. - Variations to the basic configuration.

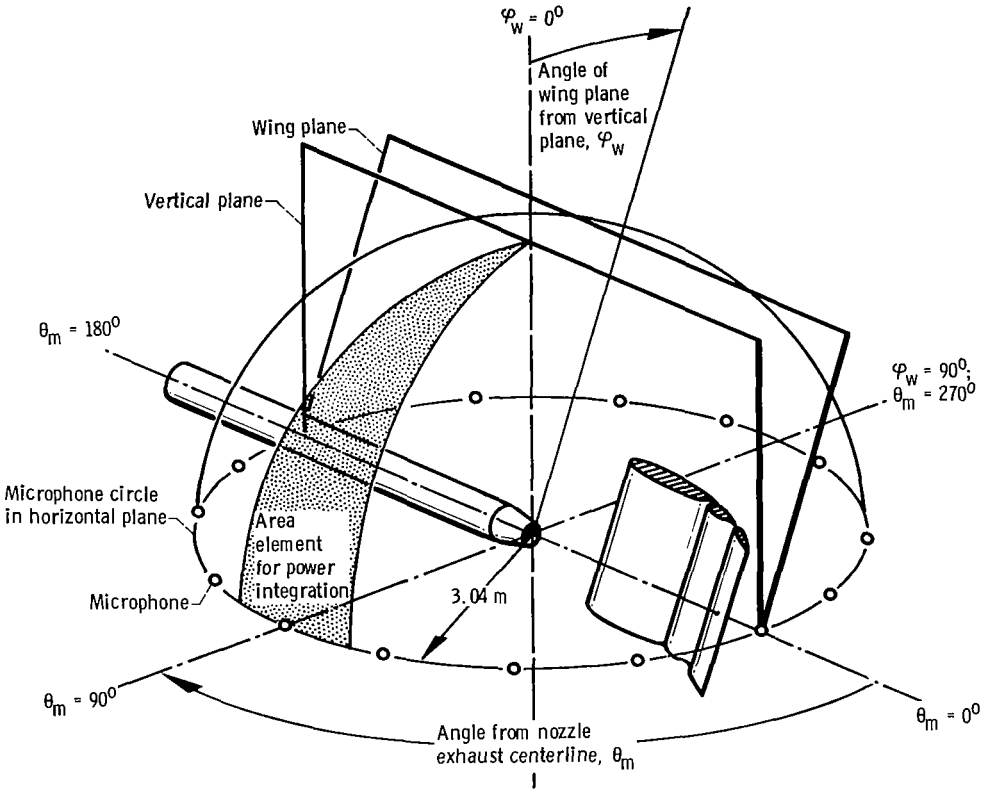

Figure 5. - Microphone setup and area element used in noise power integrations.

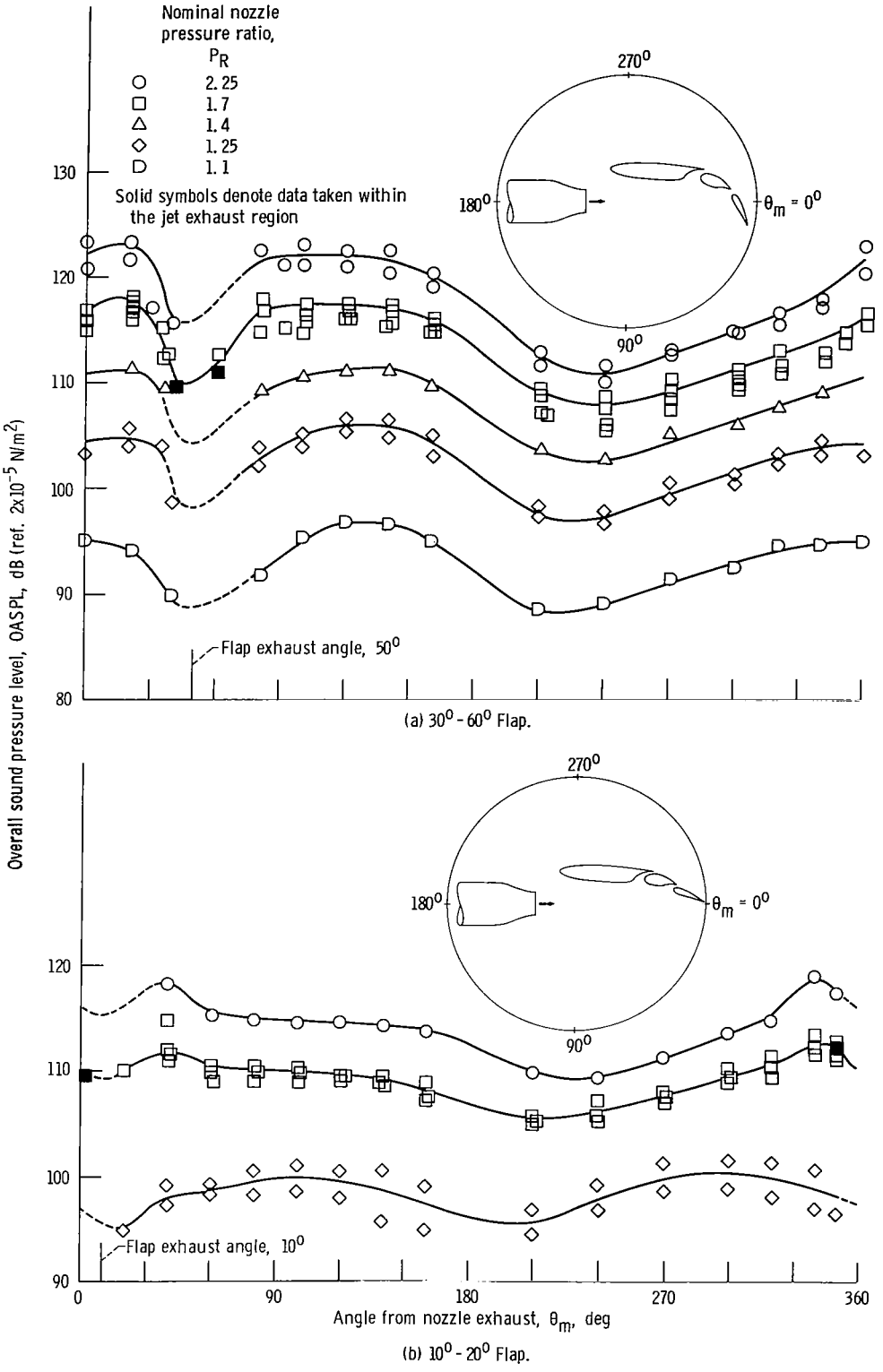

Figure 6. - Noise radiation patterns for the basic configuration. Azimuthal angle, φ_w, 0°.

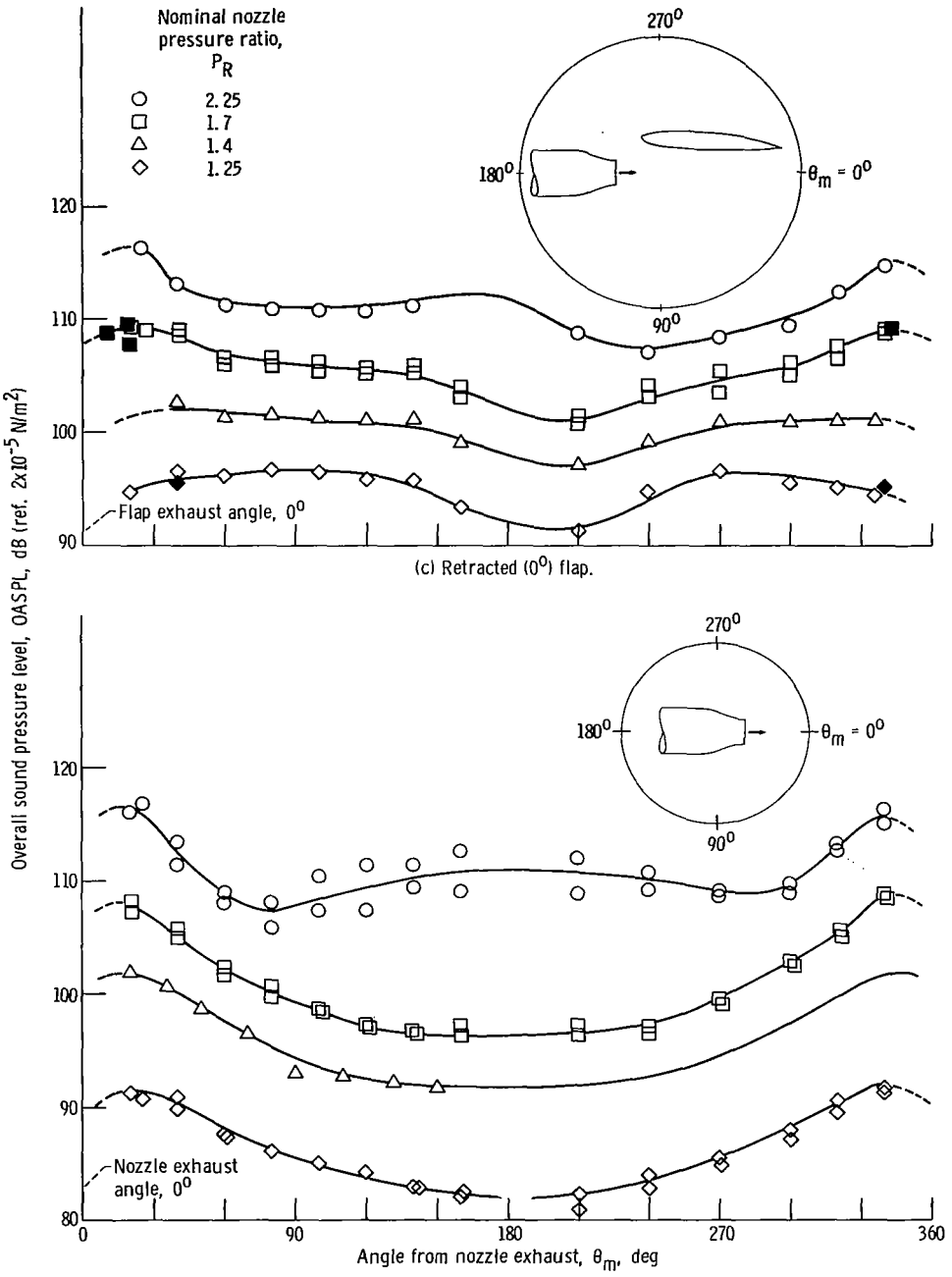

Figure 6. - Concluded.

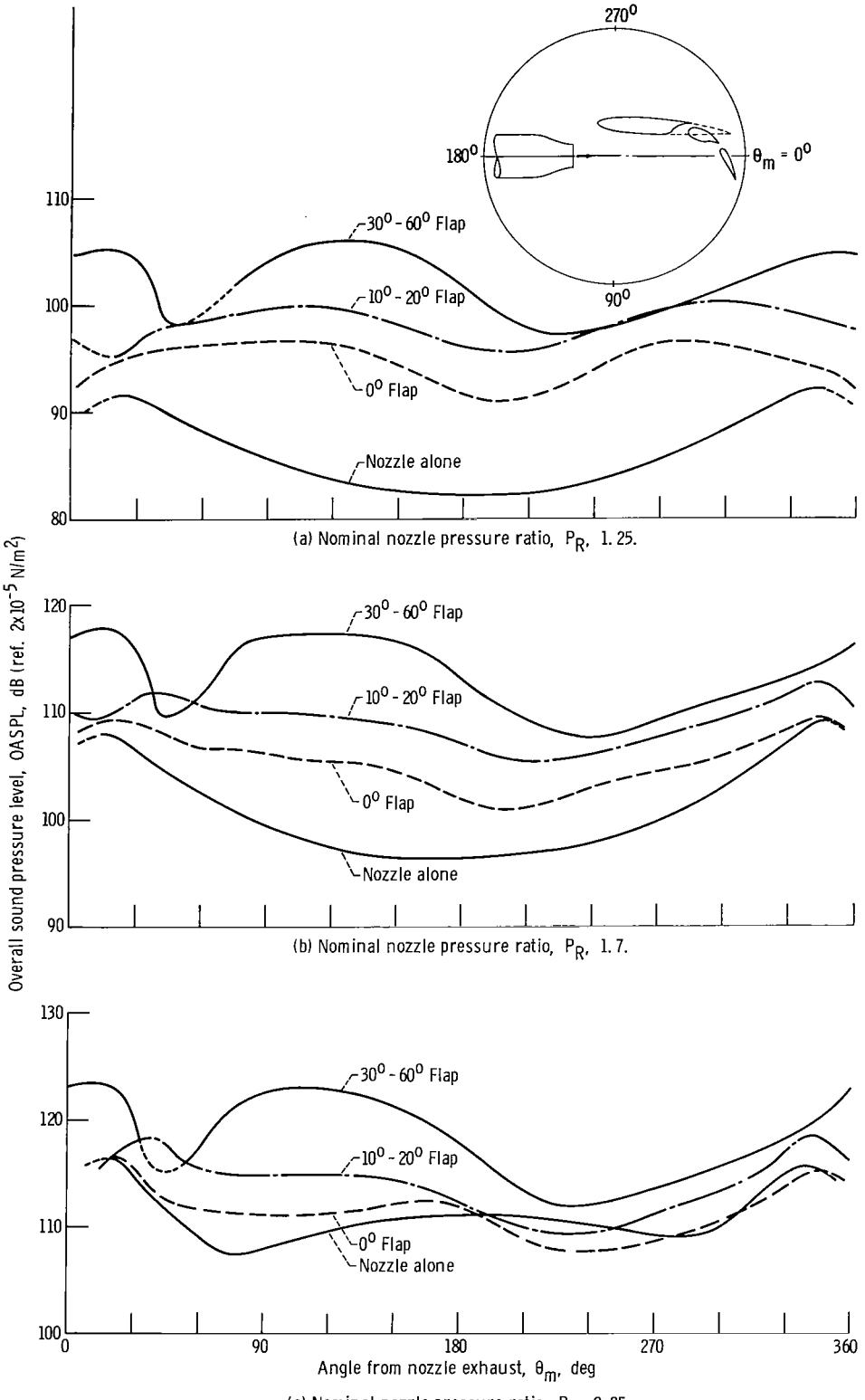

Figure 7. - Comparison of the noise radiation patterns for various flap settings of the basic configuration at a constant nominal nozzle pressure ratio. Azimuthal angle, φ_w, 0^0.

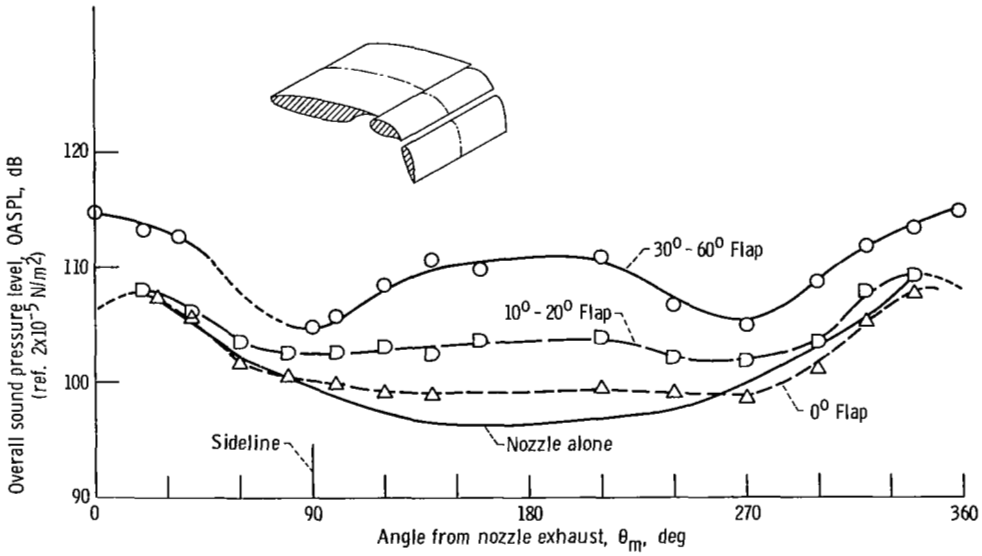

Figure 8. - Noise radiation patterns for various flap settings of the basic configuration at an azimuthal angle, φ_w, of 85^0. Nozzle pressure ratio, P_R, 1.7.

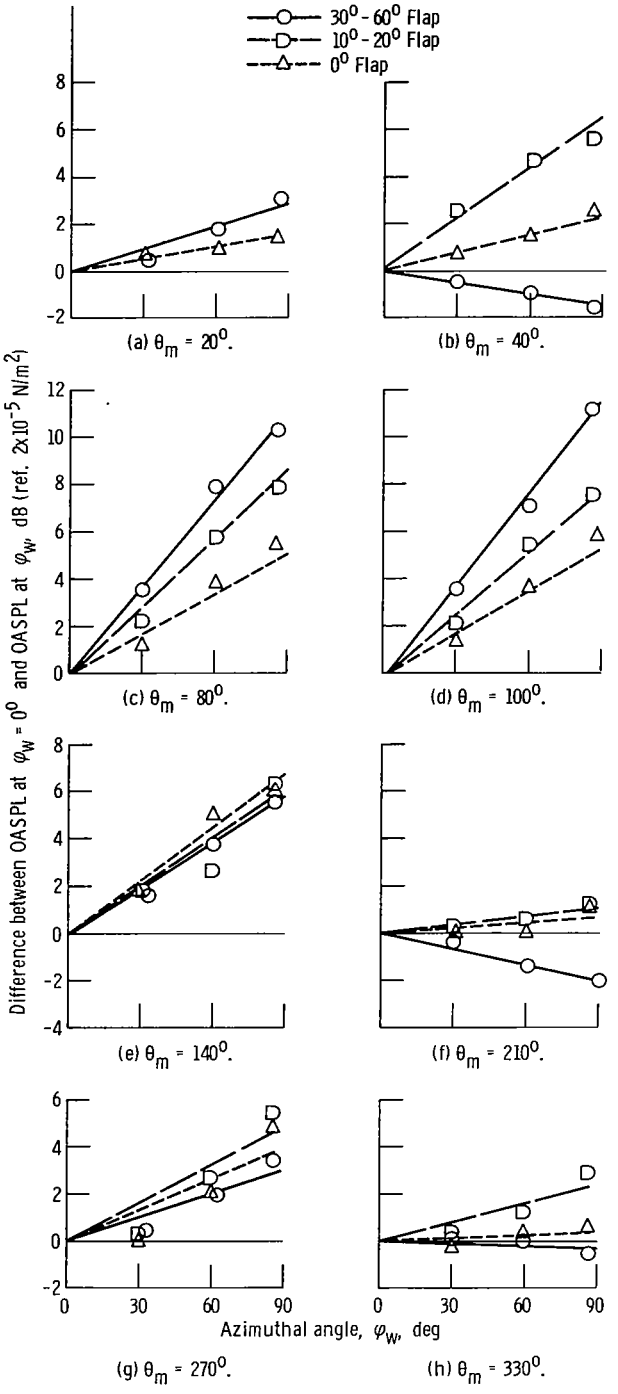

Figure 9. - Change in overall sound pressure level, OASPL, for various angles, θ_m, from the nozzle centerline. Nominal nozzle pressure ratio, P_R, 1.7.

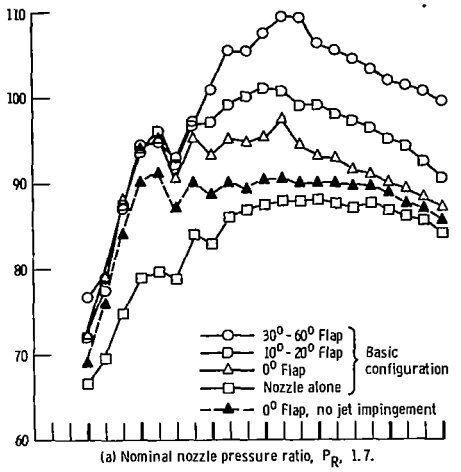

(a) Nominal nozzle pressure ratio, P_R, 1.7.

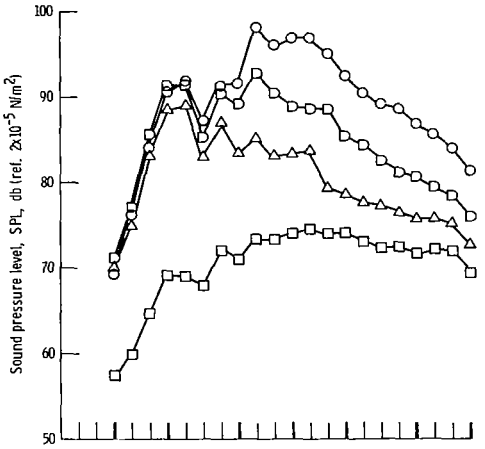

(b) Nominal nozzle pressure ratio, P_R, 1.25.

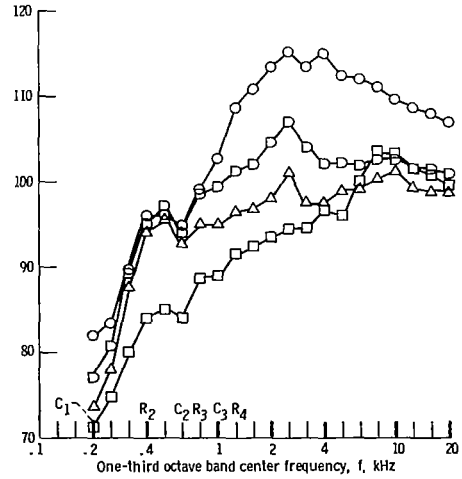

(c) Nominal nozzle pressure ratio, P_R, 2.25.

Figure 10. - One-third octave sound pressure level spectra below the wing (θ_m = 100°; φ_w = 0°) for the basic configuration. Ground-reflection cancellation and reinforcement frequencies are denoted by C_i and R_i, respectively.

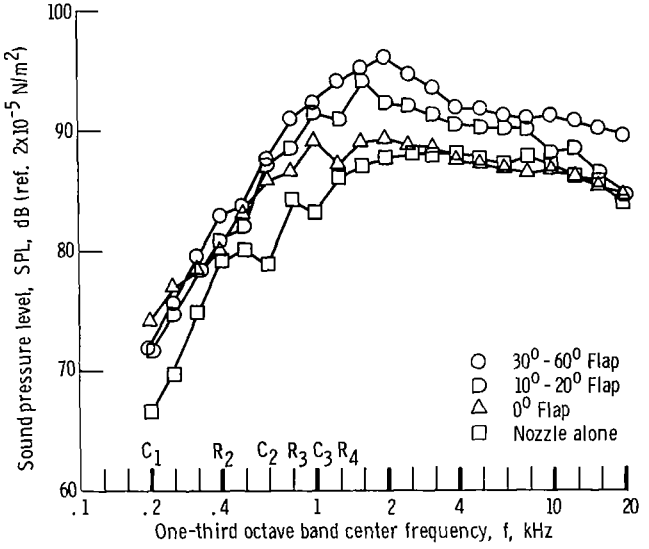

Figure 11. - One-third octave sound pressure level spectra on the sideline (θ_m = 100°; φ_w = 85°) for the basic configuration. Nominal nozzle pressure ratio, P_R, 1.7. Ground-reflection cancellation and reinforcement frequencies are denoted by C_i and R_i, respectively.

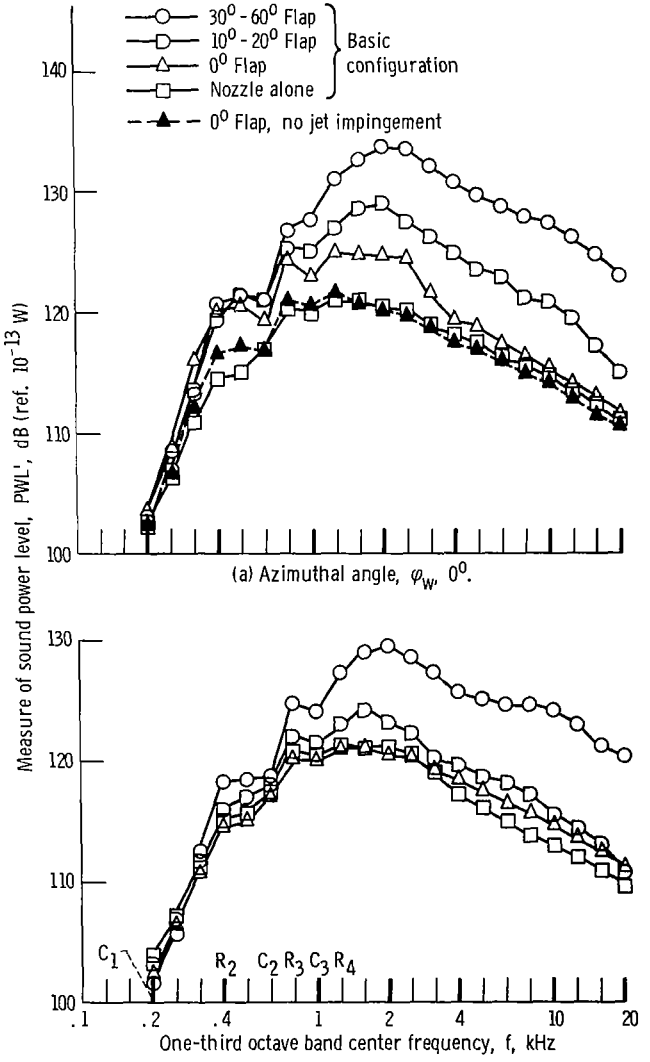

Figure 12. - One-third octave sound power level spectra for the basic configuration. Nominal nozzle pressure ratio, P_R, 1.7. Ground-reflection cancellation and reinforcement frequencies are denoted by C_i and R_i, respectively.

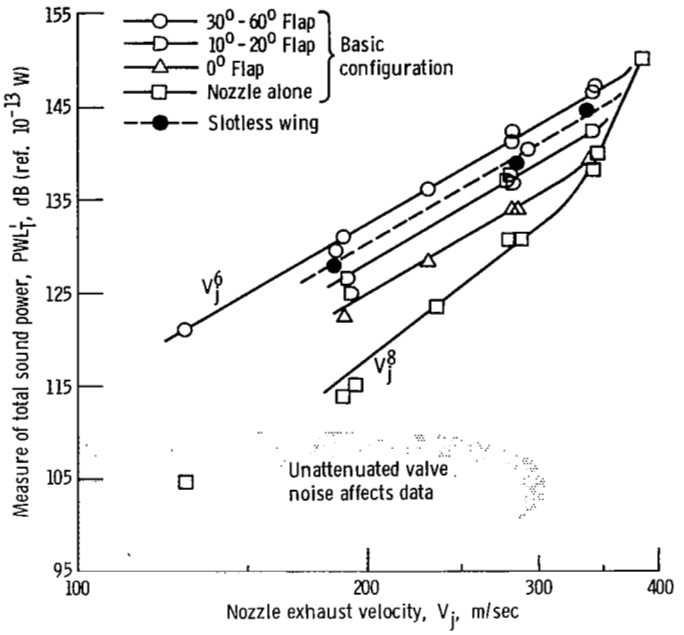

Figure 13. - Total sound power at an azimuthal angle φ_w of 0°.

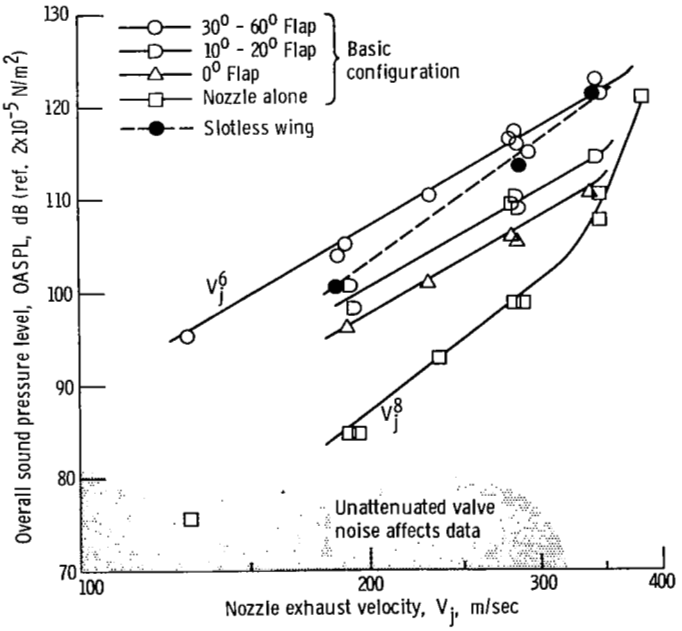

Figure 14. - Overall sound pressure level at an angular location θ_m of 100° and an azimuthal angle φ_w of 0°.

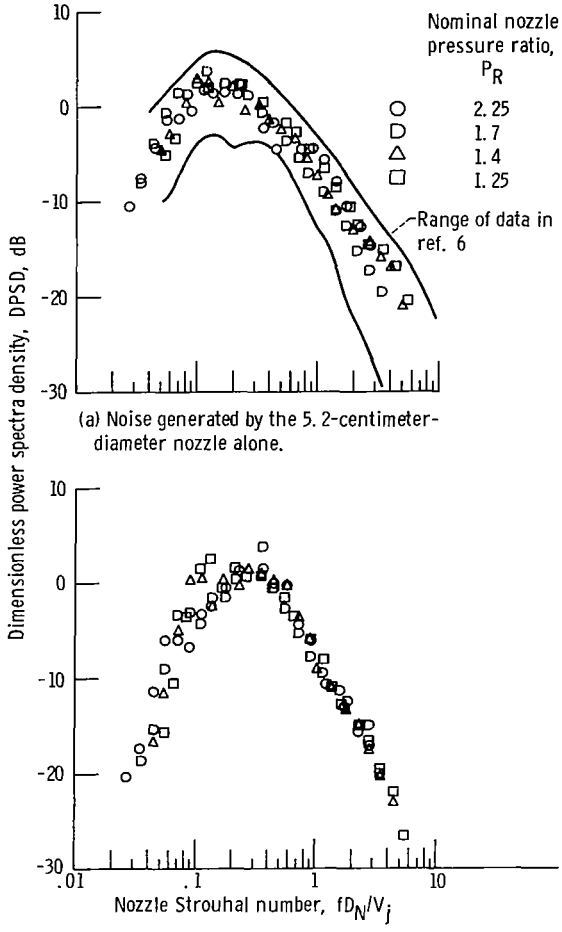

(a) Noise generated by the 5.2-centimeter-diameter nozzle alone.

(b) Noise generated by the basic configuration at the 30^0-60^0 flap position.

Figure 15. - Dimensionless power spectral density as a function of the nozzle Strouhal number. Azimuthal angle, φ_w, 0^0.

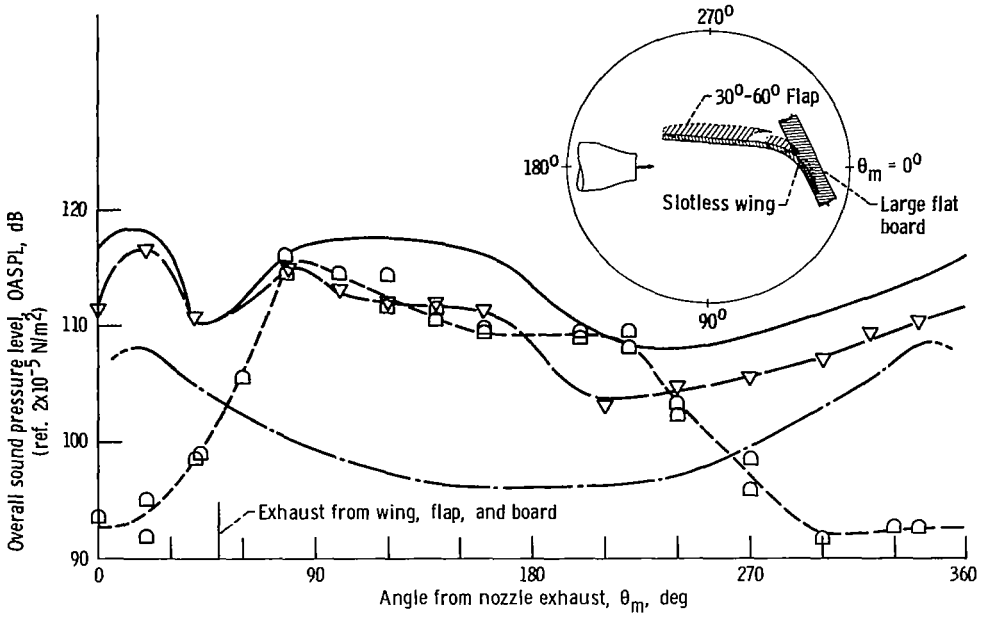

(a) Noise radiation patterns.

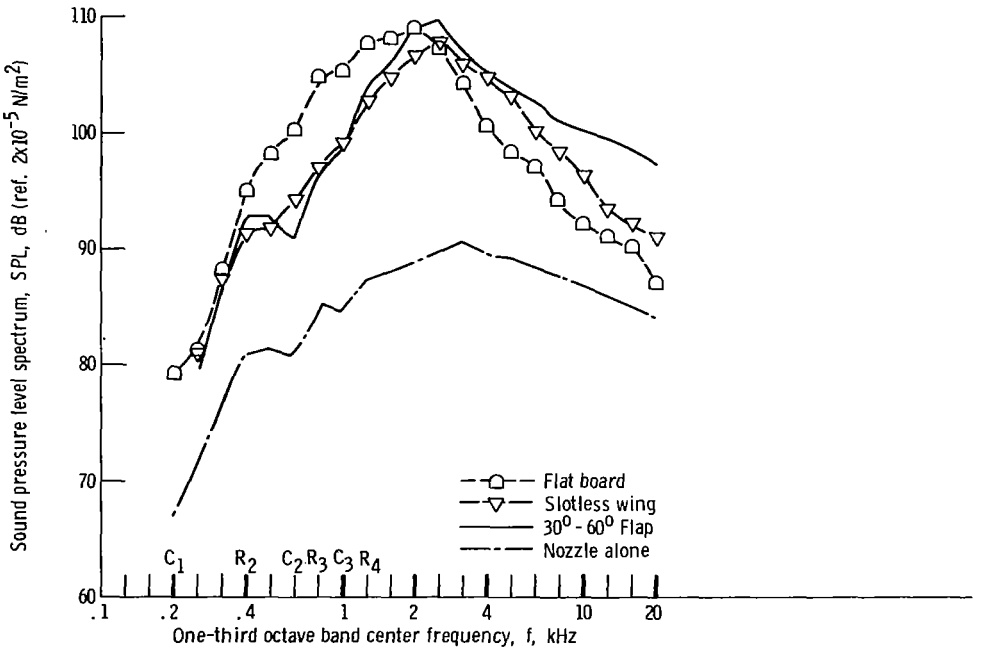

(b) Sound pressure level spectra at an angular location θ_m of 80°. Ground-reflection cancellation and reinforcement frequencies are denoted by C_i and R_i, respectively.

Figure 16. - Comparison of the noise generated by the 30° - 60° flap, the slotless wing, and the flat board. Nominal nozzle pressure ratio, P_R, 1.7; azimuthal angle, φ_w, 0°.

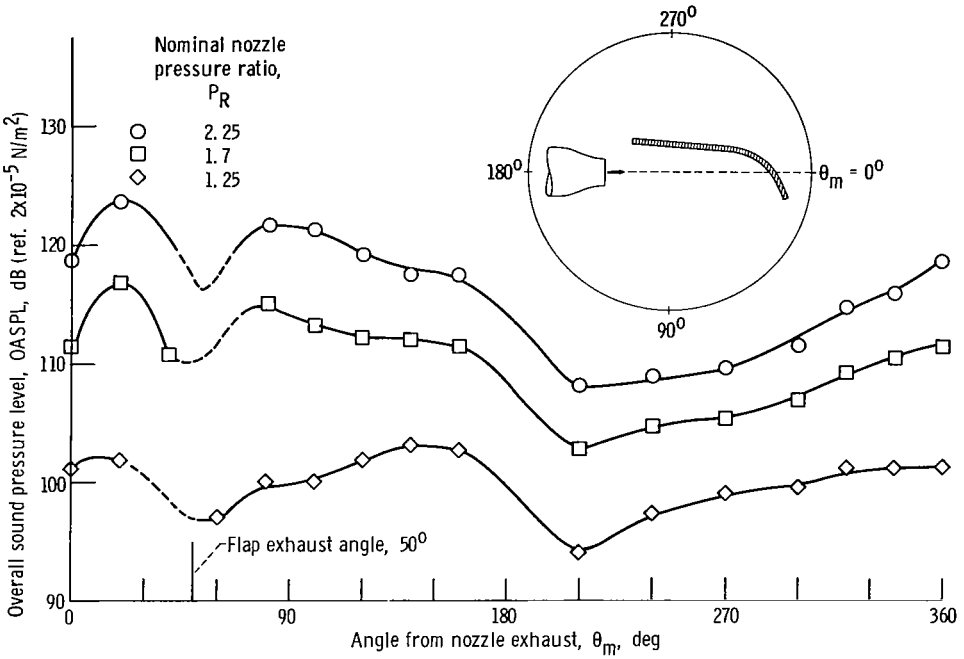

Figure 17. - Noise radiation patterns for the slotless wing.

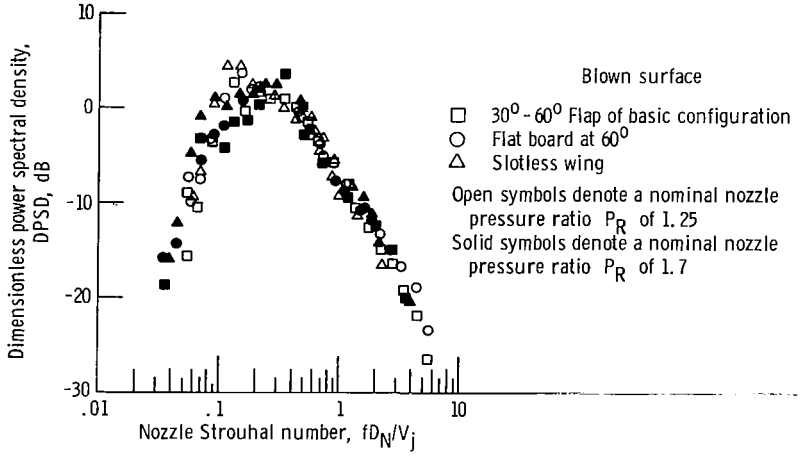

Figure 18. - Similarity of the dimensionless power spectral density curves for the noise generated by the 30° - 60° flap, the slotless wing, and the large flat board. Impingement distance, L_T, 37 cm; azimuthal angle, φ_w, 0°.

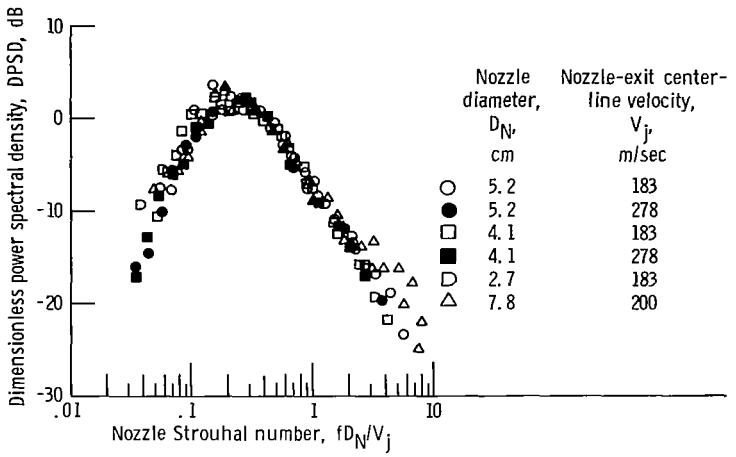

Figure 19. - Effect of nozzle diameter on the dimensionless power spectral density for the large flat board. Ratio of impingement distance to diameter, L_T/D_N, 7.05; board impingement angle, 60^0; azimuthal angle, φ_w, 0^0.

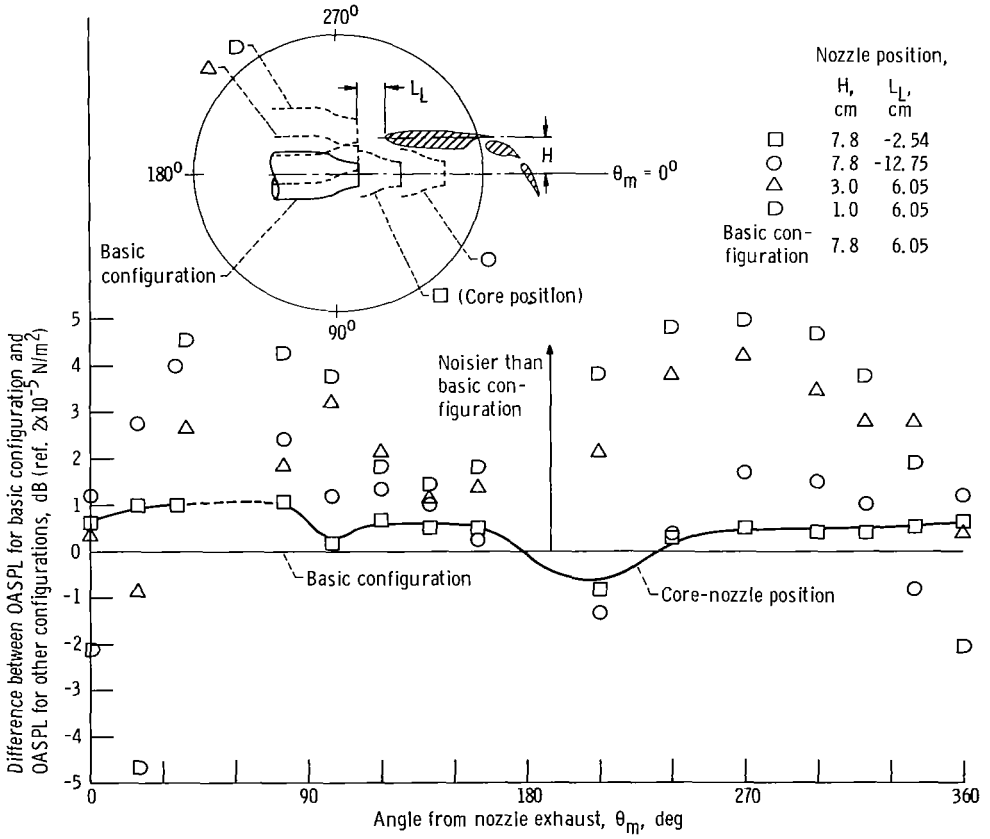

Figure 20. - Change in noise level, relative to that of the basic configuration, as the nozzle is moved closer to the wing. Nominal nozzle pressure ratio, P_R, 1.7; azimuthal angle, φ_w, 0^0.

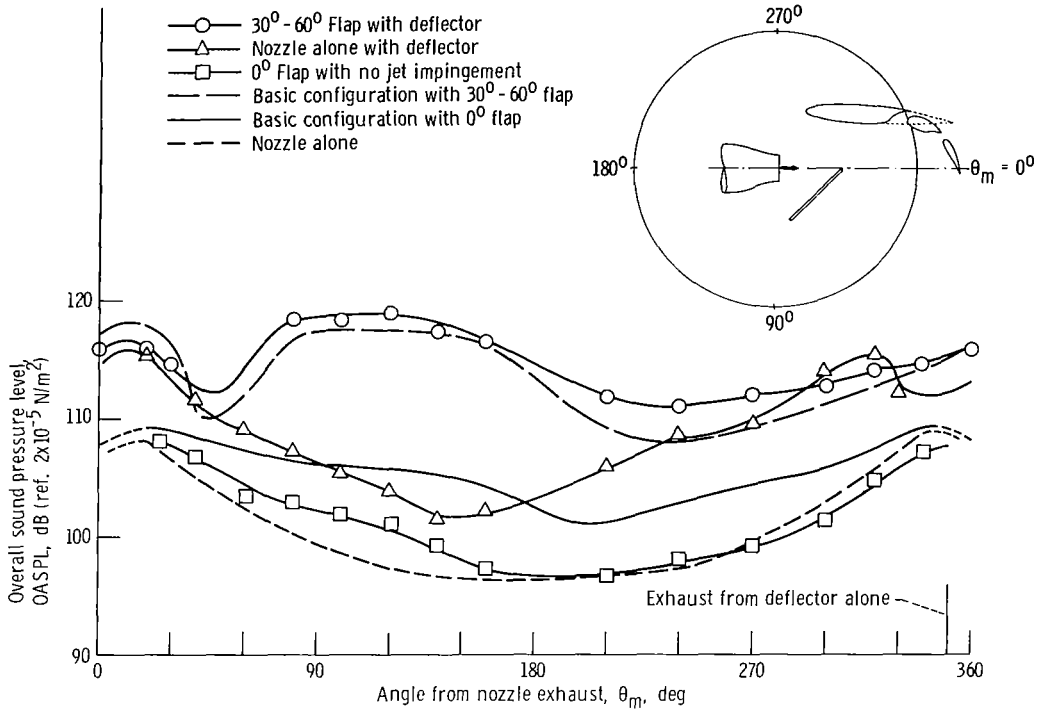

Figure 21. - Noise radiation patterns for the variations to the basic configuration that require a deflector. Nominal nozzle pressure ratio, P_R, 1.7; azimuthal angle, φ_w, 0°.

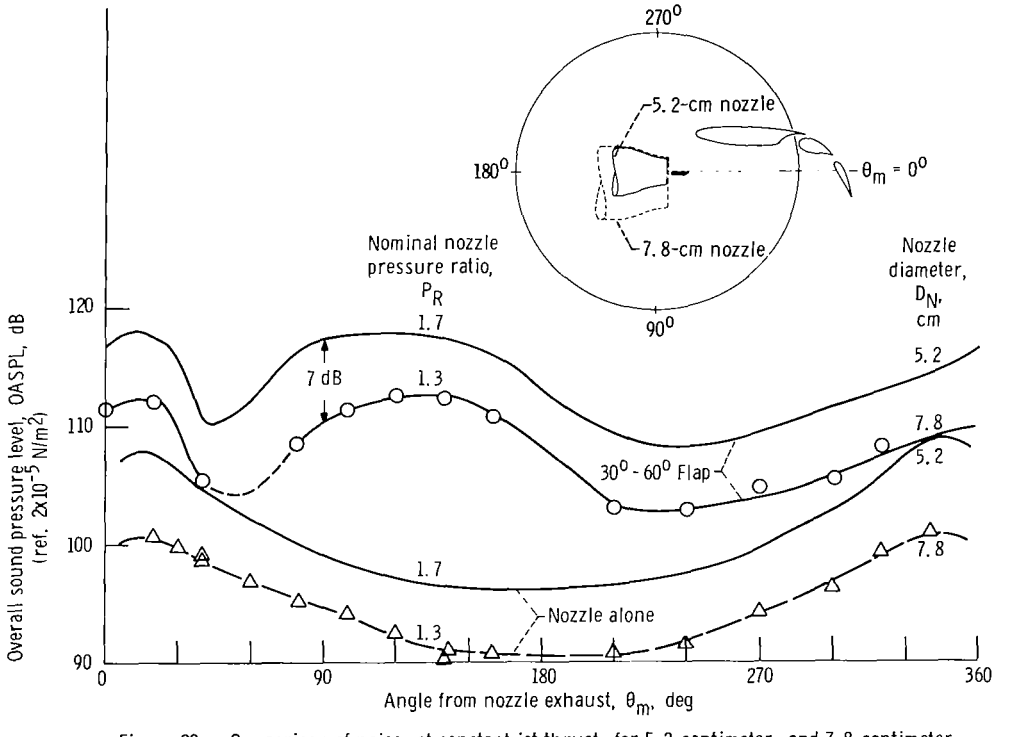

Figure 22. - Comparison of noise, at constant jet thrust, for 5.2-centimeter- and 7.8-centimeter-diameter nozzles blowing on the 30° - 60° flap. Azimuthal angle, φ_w, 0°.

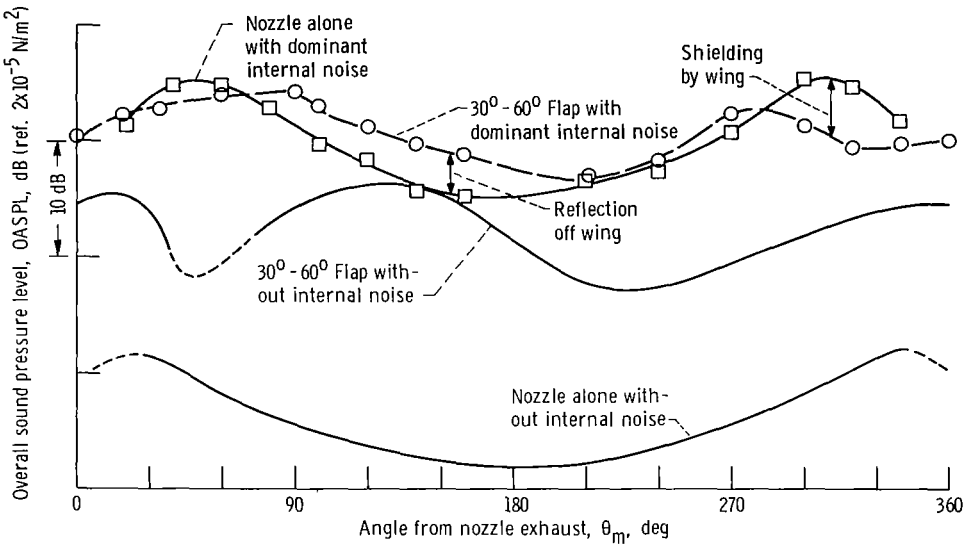

Figure 23. - Effect of a dominant internal noise on the noise patterns for the basic configuration. Nominal nozzle pressure ratio, P_R, 1.25; azimuthal angle, φ_w, 0^0.

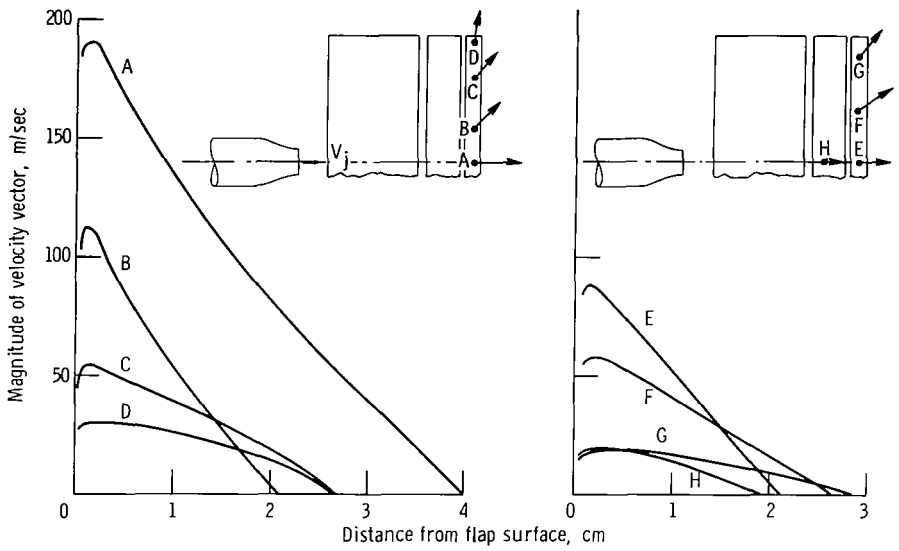

(a) Velocity vector profiles on the nozzle side of the wing.

(b) Velocity vector profiles on top of wing.

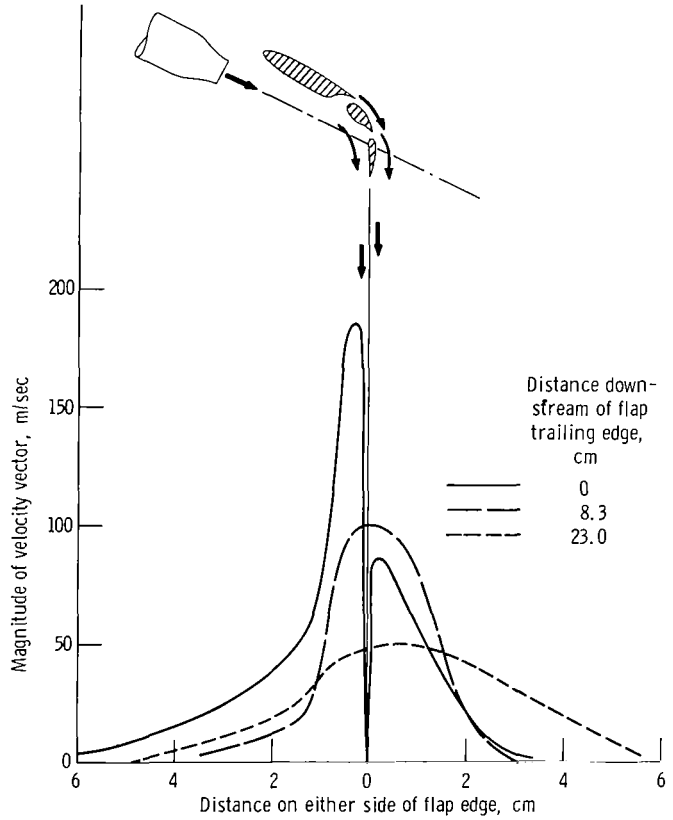

(c) Velocity profiles downstream of last flap.

Figure 24. - Flow field for the 30^0 - 60^0 flap of the basic configuration. Nozzle exhaust velocity, V_j, 190 m/sec; nominal nozzle pressure ratio, P_R, 1.25.

NASA-Langley, 1972 —— 2 E-6662